

FULL PAPER

Open Access



# $V_{S30}$ , slope, $H_{800}$ and $f_0$ : performance of various site-condition proxies in reducing ground-motion aleatory variability and predicting nonlinear site response

Boumédiène Derras<sup>1,2\*</sup> , Pierre-Yves Bard<sup>3</sup> and Fabrice Cotton<sup>4,5</sup>

## Abstract

The aim of this paper is to investigate the ability of various site-condition proxies (SCPs) to reduce ground-motion aleatory variability and evaluate how SCPs capture nonlinearity site effects. The SCPs used here are time-averaged shear-wave velocity in the top 30 m ( $V_{S30}$ ), the topographical slope (slope), the fundamental resonance frequency ( $f_0$ ) and the depth beyond which  $V_s$  exceeds 800 m/s ( $H_{800}$ ). We considered first the performance of each SCP taken alone and then the combined performance of the 6 SCP pairs [ $V_{S30}$ - $f_0$ ], [ $V_{S30}$ - $H_{800}$ ], [ $f_0$ -slope], [ $H_{800}$ -slope], [ $V_{S30}$ -slope] and [ $f_0$ - $H_{800}$ ]. This analysis is performed using a neural network approach including a random effect applied on a KiK-net subset for derivation of ground-motion prediction equations setting the relationship between various ground-motion parameters such as peak ground acceleration, peak ground velocity and pseudo-spectral acceleration PSA ( $T$ ), and  $M_w$ ,  $R_{JB}$ , focal depth and SCPs. While the choice of SCP is found to have almost no impact on the median ground-motion prediction, it does impact the level of aleatory uncertainty.  $V_{S30}$  is found to perform the best of single proxies at short periods ( $T < 0.6$  s), while  $f_0$  and  $H_{800}$  perform better at longer periods; considering SCP pairs leads to significant improvements, with particular emphasis on [ $V_{S30}$ - $H_{800}$ ] and [ $f_0$ -slope] pairs. The results also indicate significant nonlinearity on the site terms for soft sites and that the most relevant loading parameter for characterising nonlinear site response is the “stiff” spectral ordinate at the considered period.

**Keywords:** Aleatory variability, Site-condition proxies, KiK-net, Neural networks, GMPE, Nonlinear site response

## Introduction

Probabilistic seismic hazard analysis (PSHA) strongly relies on ground-motion prediction equations (GMPEs) that quantify the amplitude of ground motion as a function of distance, magnitude and site-condition proxies (SCPs). The latter are introduced to characterise the amplification effects linked to near-surface deposits. Given the variety of physical phenomena impacting the characteristics of an earthquake shaking, ground-motion models include a large degree of uncertainty. This uncertainty (especially the within-event aleatory variability)

is strongly affected by near-surface site conditions. An important question is the degree to which this scatter can be reduced by improvements in the way to account for the near-surface effects. The incorporation of those effects in GMPEs has gone through an evolution in the past years (Chiou and Youngs 2008; Seyhan et al. 2014; Derras et al. 2016). At the beginning, ground-motion models typically contained a scaling parameter based on site classification (e.g. Boore et al. 1993) or presented different models for “hard rock” and “soil” sites (e.g. Campbell 1993; Sadigh et al. 1997). Boore et al. (1997) introduced the explicit use of the time-averaged shear-wave velocity in the top 30 m ( $V_{S30}$ ).  $V_{S30}$  has become de facto a standard for the development of GMPEs and seismic hazard assessment at national and international scales. In this way, it has been observed (e.g. Borchardt

\*Correspondence: b\_derras@mail.univ-tlemcen.dz

<sup>1</sup> Risk Assessment and Management Laboratory (RISAM), Abou Bekr Belkaid University, BP 230, 13048, Chetouane, Tlemcen, Algeria  
Full list of author information is available at the end of the article

1994) that  $V_{S30}$  is a useful parameter to predict local site amplification in active tectonic regimes, especially when it is actually measured: Derras et al. (2016) showed after Chiou and Young (2008) that measuring  $V_{S30}$  allows a significant reduction in the aleatory variability.

$V_{S30}$  has certainly proved to constitute a simple and efficient SCP metric, but it also proved not to be a low-cost SCP, as it is far from being measured at all strong-motion sites throughout the world (except in Japan). For this reason, Wald and Allen (2007) and Allen and Wald (2009) have proposed to use the topographical slope (slope) from digital elevation models (DEMs) derived from remote sensing (satellite imaging) to give a first-order estimation of site classes based on  $V_{S30}$ . Many other ways to infer  $V_{S30}$  values without measuring them have been proposed, as listed in Seyhan et al. (2014): extrapolation from  $V_S$  measurements at depths shallower than 30 m, correlations—more or less robust—with other types of information or parameters (geology, geomorphological or terrain-related proxies, geotechnical parameters).

On the other hand,  $V_{S30}$  alone cannot satisfactorily predict the amplification for sites underlain by deep sediments, which require knowledge of the geology to depths greater than 30 m (e.g. Choi and Stewart 2005; Luzi et al. 2011). Campbell (1989) found that adding a parameter for depth to basement rock improved the predictive ability of empirical ground-motion models. On their side, Cadet et al. (2011) and Derras et al. (2012) used another SCP: the fundamental resonance frequency,  $f_0$ , as determined by the horizontal-to-vertical (H/V) spectral ratio technique (Mucciarelli 1998; Haghshenas et al. 2008; Bard et al. 2010). As the  $f_0$  (H/V) SCP is able to identify low-frequency amplification on thick sites, its relevance may be compared with the performance of another SCP often proposed to properly account for the sediment thickness,  $H_{800}$  (depth beyond which the shear-wave velocity exceeds 800 m/s).

The main aim of this work was to assess the actual performance of several site-condition proxies, namely  $V_{S30}$ , slope,  $f_0$  (H/V) and  $H_{800}$  SCP, by analysing the relative decrease in the ground-motion aleatory variability each of them allow to achieve and by investigating the benefits of considering simultaneously multiple site proxies. In addition, as all the considered ANN models were found to predict a significantly nonlinear site response, a secondary aim has been to investigate to which extent these SCPs allow to capture not only the linear, but also the nonlinear nature of site response, in combination with various loading parameters (PGA on rock, acceleration response spectrum at the period of interest PSA ( $T$ ), or a site-related strain proxy  $PGV/V_{S30}$ ).

The KiK-net database used here consists of shallow crustal events recorded on sites for which several site

proxies are already available:  $V_{S30}$  and  $H_{800}$  values can be directly derived from downhole measurements of  $V_S$  profile (Dawood et al. 2014), the slope values have been compiled (Ancheta et al. 2014), and  $f_0$  values are taken from Régnier et al. (2013). The KiK-net data offer the unique opportunity to have, for each strong-motion recording, a reliable measurement of the four SCPs, thus allowing a thorough and meaningful comparative assessment of the performance of each of these proxies.

The artificial neural network (ANN) approach and a random-effect-like procedure (Derras et al. 2014) have been used for the derivation of GMPEs setting the relationship between various ground-motion parameters [peak ground acceleration (PGA), peak ground velocity (PGV) and 5% damped pseudo-spectral acceleration (PSA) from 0.01 to 4 s] and event/station meta-parameters (moment magnitude  $M_w$ , Joyner and Boore distance  $R_{JB}$ , focal depth and site-condition proxies  $V_{S30}$ , slope,  $H_{800}$  and  $f_0$ ).

After a short presentation of the data set, a section is dedicated to the presentation of the ANN models and their specific implementation for deriving GMPEs. The following section presents the results obtained for the KiK-net data, focusing on (a) the respective performance of each of the four site proxies which are considered either alone or within combinations and (b) a discussion of their ability to detect and account for nonlinear site response.

## Data set

The Kiban–Kyoshin network (KiK-net) is one of the two national strong-motion seismograph networks developed in Japan following the 1995 Kobe earthquake. The KiK-net is a network of strong-motion instruments that consist of about 700 stations with an average spacing of about 20 km distributed throughout the Japanese islands (Hayashida and Tajima 2007). The KiK-net stations are each equipped with a pair of surface and downhole, sensitive three-component digital accelerometers, allowing an empirical evaluation of the site response at each station.

The resulting data set considered here has been compiled by Dawood et al. (2014, 2016). This data set has been downloaded from <https://datacenterhub.org/resources/272>. The corresponding data processing is fully described in Dawood et al. (2014, 2016). In short, this data processing includes several steps: baseline correction, tapering on both ends (total length of tapering = 5% of the total record length), zero padding before and after recommended by Boore (2005) in relation to the order and frequency of the high-pass filtering, fourth-order acausal Butterworth filtering with selection of the cut-off frequency  $f_c$  so that the computed final velocity and

displacement values at the end of the time series remain smaller than some magnitude-dependent thresholds, signal-to-noise ratio larger than 3 between  $2 f_c$  and 30 Hz.

The data set using here contains 977 recordings from 199 sites to 214 earthquakes. The range of  $M_w$ ,  $R_{JB}$ , depth and all SCPs is listed in Table 1, which also provides the number of earthquakes, records and sites. The corresponding range of recorded PGA values spans from  $2.6 \times 10^{-4}$  to 0.41 g.

#### Site-condition proxies

The chosen site proxies are  $V_{S30}$  and slope, which are generally considered a priori as more relevant for short-period ground motions, and  $f_0$  (H/V) and  $H_{800}$ , that should in principle be more suitable for long periods. There actually exist several possibilities proposed by different authors for such a sediment thickness parameter. It is true that most recent NGA-West and NGA-West 2 GMPEs use depths corresponding to larger velocities, as indicated by the reviewer. We have chosen to select  $H_{800}$  as a thickness parameter for the following reasons:

- The database used in this study provides only the  $H_{800}$  values.  $H_{2500}$  and  $H_{1100}$  values are not available yet in this database.
- The ongoing revision of European building codes recommends the use of both  $V_{S30}$  and  $H_{800}$  for site classification, since the “rock” sites are conventionally associated with  $V_{S30}$  values exceeding 800 m/s. Results associated with  $H_{800}$  are then of interest of many colleagues.

The larger the target velocity, the larger the uncertainty on the corresponding depth: even in very well-known areas such as California, the different existing models lead to highly variable  $H_{2500}$  values (see Figure 10 in Seyhan et al. 2014).  $H_{800}$  thus seems an acceptable compromise, especially as we do not look for “basin” effects (i.e. including 2D or 3D very-low-frequency effects, such as

those existing in the Los Angeles area or Kanto plain), but simply for a parameter that helps to constrain the intermediate response (around 1 s).

Ground-motion models are derived first using one single SCP [one model with each of the four values:  $V_{S30}$  or slope or  $f_0$  or  $H_{800}$ ] and then using two SCPs out of the four [i.e. six models in total with the six pairs ( $V_{S30}$ , slope), ( $V_{S30}$ ,  $H_{800}$ ), ( $V_{S30}$ ,  $f_0$ ), ( $H_{800}$ , slope), ( $f_0$ ,  $H_{800}$ ) and (slope,  $f_0$ )]. All SCPs are considered through their  $\log_{10}$  values. In addition, two reference ground-motion models are established for comparison with each of the 10 previous ones: the first one is without any site proxy (named “without site proxy”), and the second one considers simultaneously all four site proxies (named “all proxies”) to estimate the maximum possible standard deviation reduction.

#### Data distribution

The distribution of the data set according to  $M_w$ ,  $R_{JB}$ , focal depth, PGA and site-condition proxy (SCP) is displayed in Figs. 1 and 2.

Figure 1 shows the distributions of the KiK-net data set in the magnitude–distance plane by bins of PGA and in the PGA–distance plane by bins of  $M_w$ . The distributions are given for all site conditions (left column), but also for soft sites only ( $V_{S30} < 300$  m/s, middle column) and stiff sites only ( $V_{S30} > 800$  m/s, right column). The goal of these presentations by bins of  $M_w$ , PGA and  $V_{S30}$  is to ensure that the data distribution is appropriate for all  $M_w$ –PGA and for soft and stiff soils. This figure also illustrates clearly the much smaller number of recordings at distances less than 10 km in general and less than 30 km when only stiff-to-rock sites are considered.

Figure 2 represents the cumulative distribution function (CDF) of the used data set versus  $R_{JB}$ ,  $M_w$ ,  $V_{S30}$ , topographical slope,  $H_{800}$ ,  $f_0$ , focal depth and PGA. The four SCP distributions are found to follow a lognormal distribution as well as  $R_{JB}$  and PGA, while  $M_w$  and focal depth are much closer to a normal distribution (see also

**Table 1** Range of magnitude, distance and site-condition proxy for the KiK-net subset considered in this study

Metadata parameters	Parameters range		Total number of earthquakes	Total number of recordings	Total number of sites
	Min	Max			
$M_w$	3.7	6.9	214	977	199
$R_{JB}$ (km)	3.65	440.63			
Depth (km)	0.00	30.00			
$V_{S30}$ (m/s)	152.94	1432.8			
$f_0$ (Hz)	0.22	22.72			
$H_{800}$ (m)	1	550			
Slope (m/m)	0.0025	0.3748			

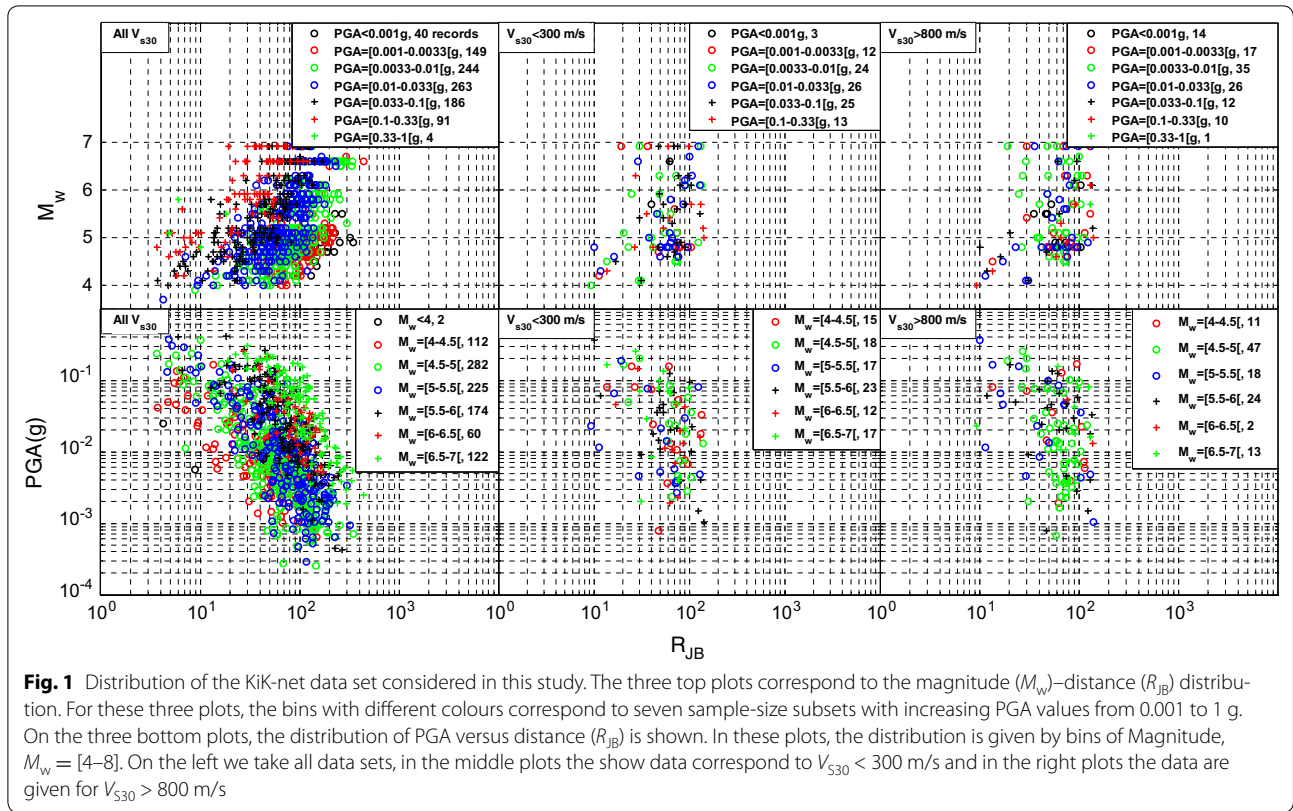


Figure 2 in Derras et al. 2016). In our ANN models, we thus used the logarithm (base 10) values of all SCPs and spectral ordinates PSAs. Table 2 details a fractile values for each of these metadata parameters: median value, 5 and 95% fractiles which are considered to provide the range of applicability of the models, and the 10 and 90% fractiles which will be used in the following to estimate the impact of each SCP on the site amplification factor.

To ensure that the SCPs are not strongly dependent on one another, correlation plots are displayed for each pair of SCPs (Fig. 3) together with the corresponding correlation coefficient ( $R$ ). Although some pairs do exhibit some correlation ( $R_{max} = 0.55$  between  $V_{530}$  and  $f_0$ ), the scatter is large enough for the SCPs to be considered as almost independent site parameters for the derived ANN models. The weakest correlation is found between slope and either  $H_{800}$  or  $f_0$ . One may notice that  $H_{800}$  is negatively correlated with the three other SCPs: the larger it is, the lower are  $f_0$ ,  $V_{530}$  and slope—as could be intuitively expected. In the same figure are also indicated the median values and the 10 and 90% fractiles for the all SCPs.

**Methods**

The random-effect regression algorithm made popular within engineering seismology by Abrahamson

and Youngs (1992), which is arguably the most commonly used approach for developing empirical ground-motion models. In our ANN models, we used this type of approach in order to facilitate the comparability with classical GMPEs. The ANN has the advantage that no prior functional form is needed (Derras et al. 2012): the actual dependence is established directly from the data and can therefore be used as a guide for a better understanding of the factors which control ground motions. This resulted in a two-phase building process.

**Fixed models**

The architecture of ANN used in this work is named “feedforward network”, consisting of a series of layers. The first layer ensures the connection with the input parameters, i.e. in our case  $M_w$ ,  $R_{JB}$  and depth and one or two (or possibly more) continuous parameter describing the SCPs ( $V_{530}$ , slope,  $f_0$ ,  $H_{800}$ ). Each subsequent layer has a connection from the previous layer. The final layer produces the network’s output. A feedforward network with one hidden layer and three neurons in the hidden layer is adopted in this study. This small number of hidden neurons is the optimal number in order to optimise both the total standard deviation of residuals  $\sigma$  and the Akaike information criterion (Akaike 1973). Figure 4 illustrates a typical architecture of the ANN-fixed models

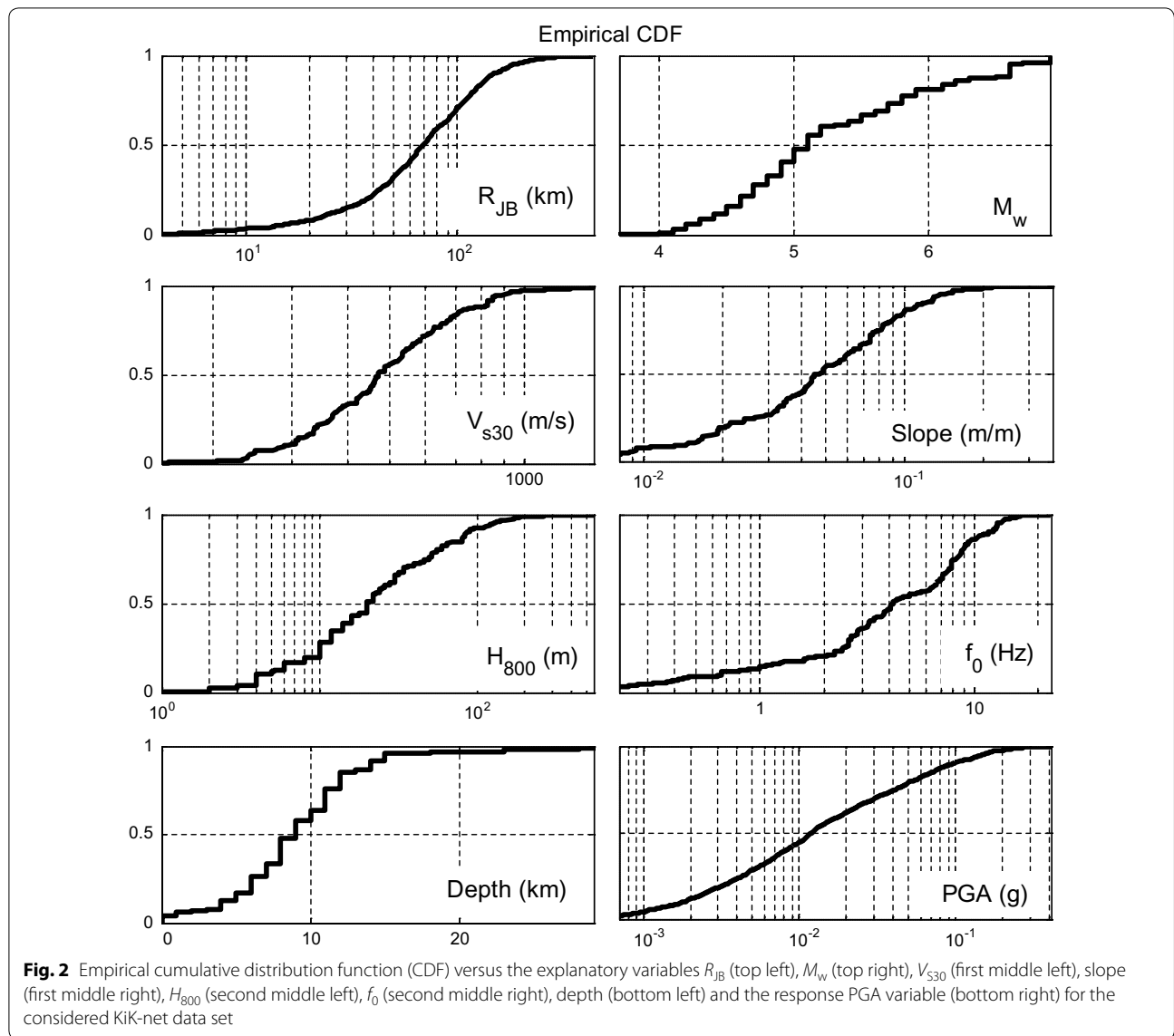


**Table 2 Metadata range for site effect analysis and for fully data-driven models applicability**

Metadata parameters	CDF (%)				
	Median	Range of applicability of fully data-driven models		Extreme values for site effect analysis	
	50%	05%	95%	10%	90%
$V_{s30}$ (m/s)	468	243	900	289	829
$f_0$ (Hz)	4.2	0.32	13	0.66	11.71
$H_{800}$ (m)	20	4	128	4	86
Slope (m/m)	0.045	0.009	0.136	0.015	0.117
$M_w$	5.1	4.2	6.6	4.4	6.6
$R_{JB}$ (km)	68.5	13.8	184.2	22.9	148.3
Depth (km)	9	1	15	4	14

which were implemented within the MATLAB® Neural Network Toolbox™ (Demuth et al. 2009). The output layer groups all the considered ground-motion parameters, i.e. the classical geometric mean of the horizontal components of PGA, PGV and 5%-damped PSA at 18 periods from 0.01 to 4 s. We did not include predictions for peak ground displacement (PGD), which we consider to be too sensitive to the high-pass filters used in the data processing.

Quasi-Newton back-propagation technique also called “BFGS” (Broyden–Fletcher–Goldfarb–Shanno) has been applied for the training phase (Shanno and Kettler 1970). To avoid “overfitting” problems, we chose an adequate regularisation method involving the modification of the conventional mean sum of the squares of the network errors by the addition of a term equal to the sum of the



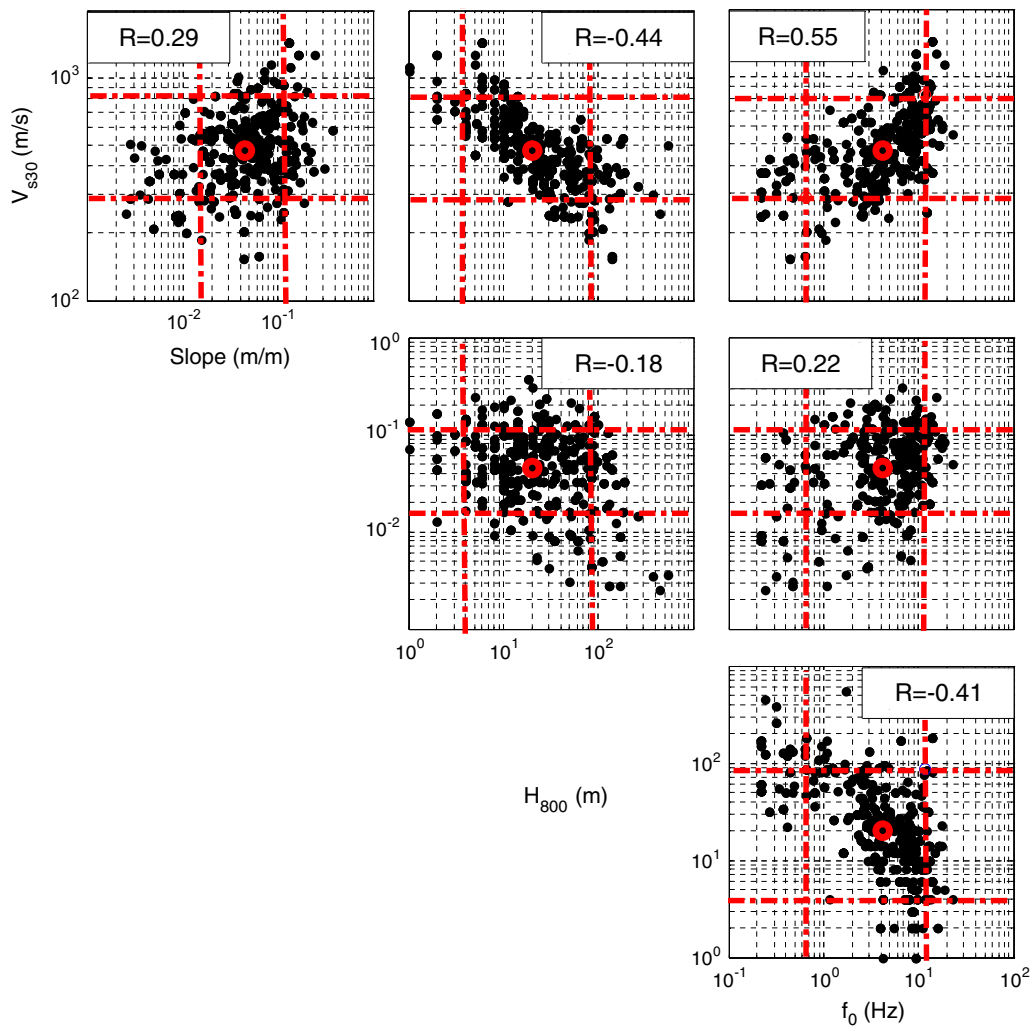


**Fig. 3** Correlation between the different SCPs, with the correlation coefficient values for each pair of SCPs. The dotted line represents the extreme values of the PCS: 10 and 90% of the empirical CDF, respectively. The red circles present the SCPs median values. The extreme and median values are presented in Table 2

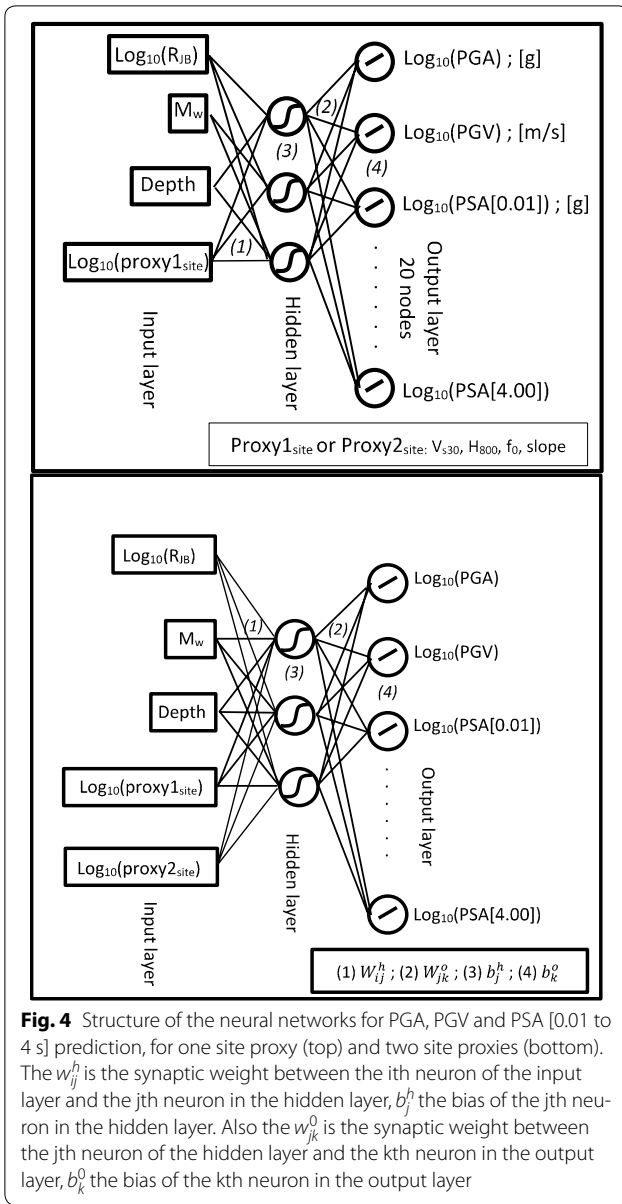
squares of the network synaptic weights and bias (Derras et al. 2012, 2014). Moreover, the optimal activation functions were found to be a “tangent sigmoid” for the hidden layer and “linear” for the output layer.

Fully data-driven GMPEs were developed, differing by the nature of parameters used in the input layer. The first ANN model is built on the basis of the  $M_w$ ,  $R_B$  and focal depth as inputs: it accounts only for source and path effects and sets the reference to quantify the gains achieved by the consideration of the various site proxies in the other ANN models. The second pack of four ANN models considers only one SCP in the input layer, namely  $V_{S30}$ , slope,  $H_{800}$  and  $f_0$  (proxy1<sub>site</sub> in Fig. 4). The next six ANN models investigate the combined influence

of pairs of SCPs (proxy1<sub>site</sub> and proxy2<sub>site</sub> in Fig. 4). Finally, another set of four ANN models combining three SCPs as input parameters and one ANN model accounting simultaneously for the four SCPs are developed to provide an estimate of the maximum improvement (i.e. reduction in the standard deviation of residuals), which may be reached with the four considered site proxies.

#### Random-effect model

A procedure similar to the random-effect approach was then used to provide the between- and within-event sigma, as described in Derras et al. (2014). For each of all the considered cases, the final ANN model is obtained using the maximum likelihood approach developed by



Brillinger and Preisler (1985) and stabilised by Abrahamson and Youngs (1992). The performance of the ANN scheme is measured by the  $\sigma$  value classically used in GMPEs, which is decomposed into the between-event ( $\tau$ ) and within-event ( $\phi$ ) variabilities: both are zero-mean, independent, normally distributed random variables with standard deviations  $\tau$  and  $\phi$  (Al Atik et al. 2010). The between- and within-event residuals are assumed uncorrelated, so that the total  $\sigma$  at a period  $T$  of the ground-motion model can be calculated according to Eq. 1.

$$\sigma(T) = \sqrt{\tau(T)^2 + \phi(T)^2} \quad (1)$$

## Results

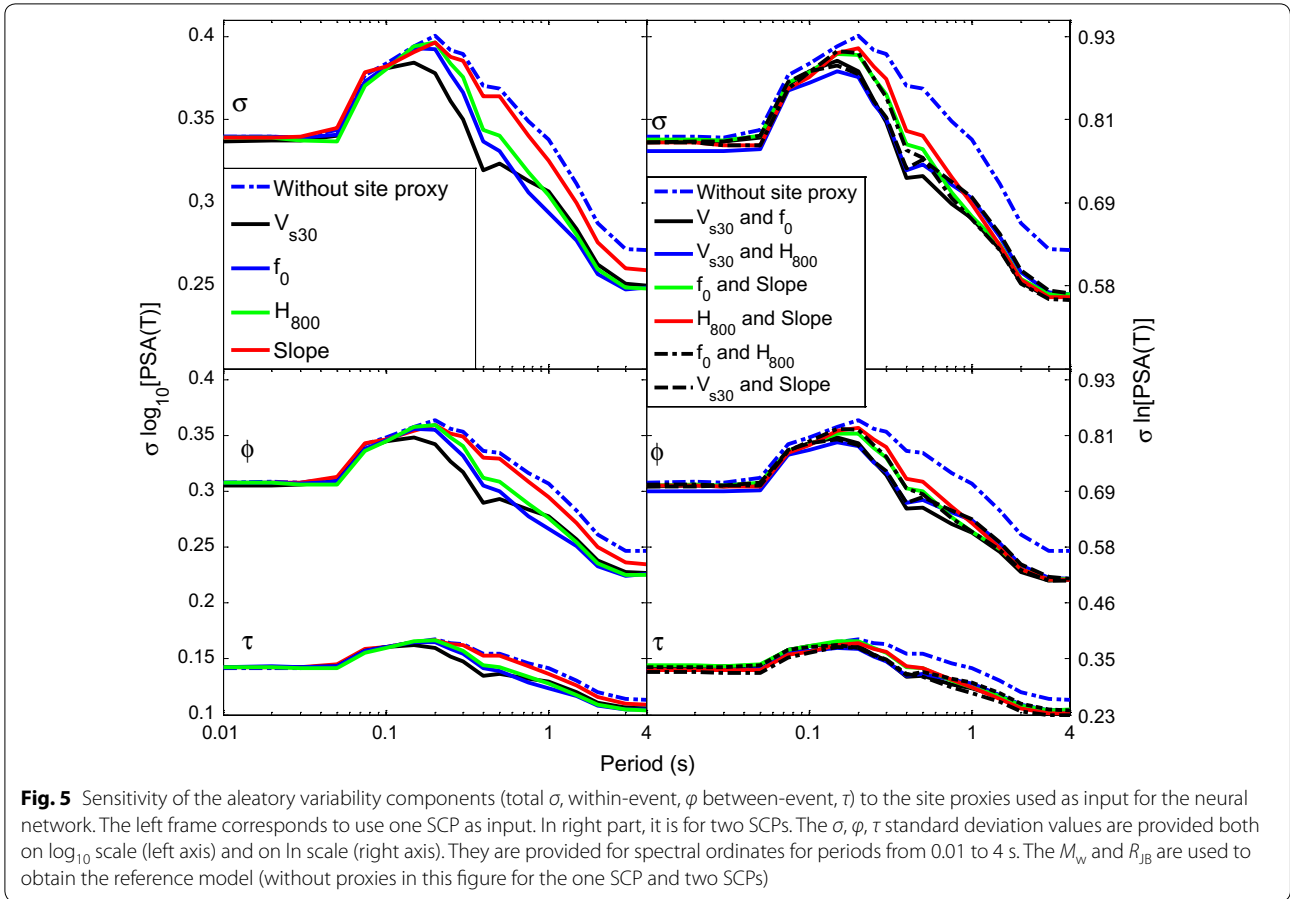
### Performance of SCPs in reducing the aleatory variability

In this section, we compare the various models derived for KiK-net data set and analyse how the various SCPs reduce the ground-motion aleatory variability. The variations of  $\tau$ ,  $\phi$  and  $\sigma$  versus period are displayed in Fig. 5 for all ANN models: without SCPs, one SCP and two SCPs.

Figure 5 shows that the between-event variability ( $\tau$ ) is much lower than the within-event variability ( $\phi$ ), which is consistent with the vast majority of previous GMPE models results. The total variability ( $\sigma$ ) is found identical at very short period ( $T < 0.05$  s) whatever the ANN model: none of the SCP is really efficient at high frequency. The various variability components then increase from 0.05 to about 0.15 s and then decrease significantly as period is increasing. A peak around 0.1 s has already been observed by some NGA-West2 GMPEs developers (e.g. Chiou and Youngs 2014; Derras et al. 2016). A possible explanation is the interaction of varying stress drop with the high-frequency damping term ( $\kappa$ ). At short-to-intermediate periods, i.e. for  $T$  between 0.1 and 0.6 s, one-SCP models allow reducing the within-event standard deviation compared to the reference model. The smallest  $\phi$  is obtained for the  $V_{S30}$  SCP, followed by  $f_0$  and  $H_{800}$  proxies, which have comparable performance, while the slope proxy exhibits the poorest performance. At longer periods,  $f_0$  and  $H_{800}$  provide the lowest  $\phi$  values and perform better than  $V_{S30}$ .

As expected, the two-SCP models lead to larger variance reductions, but it is interesting to notice than all pairs of proxies exhibit very similar performance. At short-to-intermediate periods, i.e. from 0.4 to 0.8 s, the [ $V_{S30}, f_0$ ] pair is found to provide the smallest values of  $\phi$ , while for  $T > 0.8$  s the “best” pair turns out to be [ $f_0, H_{800}$ ] as logically expected since both parameters are more sensitive to the bedrock depth. Interestingly enough, the [ $f_0, \text{slope}$ ] pair exhibits a relatively good performance over the whole period range [0.1–4 s], while it is associated with the lowest measurement cost.

In addition, to better quantify the gains achieved by each SCP (s) model, the values of the variance reduction coefficients  $R_\sigma$ ,  $R_\phi$  and  $R_\tau$  defined in Eq. 2 are presented in Fig. 6. The variations of these coefficients versus period are displayed in Fig. 6 for all ANN models: without SCPs, one-SCP, two-SCP, the best three-SCP model and the single four-SCP models. The reason for which we add these three and four SCPs cases is to obtain an estimate of the maximum possible variance reduction when many site parameters are known. The  $R_\sigma$  values are also listed in Table 3 for a limited set of ground-motion parameters (PGA, PGV and PSA at  $T = [0.2, 0.5, 1.0, 2.0]$  s).



$$\begin{cases} R_{\sigma}(T) = \left(1 - \frac{\sigma_{SCP}^2(T)}{\sigma_{\text{without proxies}}^2(T)}\right) \cdot 100; (\%) \\ R_{\tau}(T) = \left(1 - \frac{\tau_{SCP}^2(T)}{\tau_{\text{without proxies}}^2(T)}\right) \cdot 100; (\%) \\ R_{\phi}(T) = \left(1 - \frac{\phi_{SCP}^2(T)}{\phi_{\text{without proxies}}^2(T)}\right) \cdot 100; (\%) \end{cases} \quad (2)$$

The obtained results confirm that the reduction in the aleatory variability becomes significant beyond  $T = 0.1$  s and for PGV as well (Table 3). For the short periods [0.1–0.6 s], the best is  $V_{S30}$ —with a maximum of 25% variance reduction at 0.4 s—while  $f_0$  outperform in the [0.6, 4] s. The variance reduction obtained with the slope SCP is the lowest of all SCPs (except between 0.1 and 0.2 s) and reaches a maximum of 9% at 4 s.  $V_{S30}$  is thus confirmed to be relevant mainly for short-to-intermediate periods, as expected from the fact that it samples only the shallow subsurface, while  $f_0$  and  $H_{800}$  are more sensitive to the deep sediments and more relevant for long periods. Similarly, the “two-SCP” models exhibit a slightly larger variance reduction at short-to-intermediate period when they include  $V_{S30}$  as one of the two site proxies (the best

performance being achieved by the  $[V_{S30}, f_0]$  pair), while the largest reduction at long periods is observed for the  $[f_0, H_{800}]$  pair, i.e. a combination of two long-period proxies, with a value of  $R_{\sigma}$  reaching 24% at  $T = 2.0$  s. Overall, the largest reduction is observed for the “reference” model accounting simultaneously for the four SCPs, followed by the three best SCPs model combining the use of  $[V_{S30}, f_0, H_{800}]$ ; it is noteworthy, however, that such “maximum possible” variance reduction does not exceed 1.5% for PGA (Table 3) and 4% for short periods around 0.08 s, while it reaches 29% around 0.4 s. The values of these variance reduction coefficients confirm that no site proxy can be preferred over the whole frequency range.

It is worth noticing in Figs. 5 and 6 that site proxies also influence the between-event standard deviation  $\tau$  in a very similar way they affect the within-event variability: it could be interpreted as resulting from the fact that a better site description enables a better description of the actual dependence of the dependence on the source and path parameters. It may also indicate that despite the random-effect procedure, the within- and between-event variabilities are not completely independent. Such



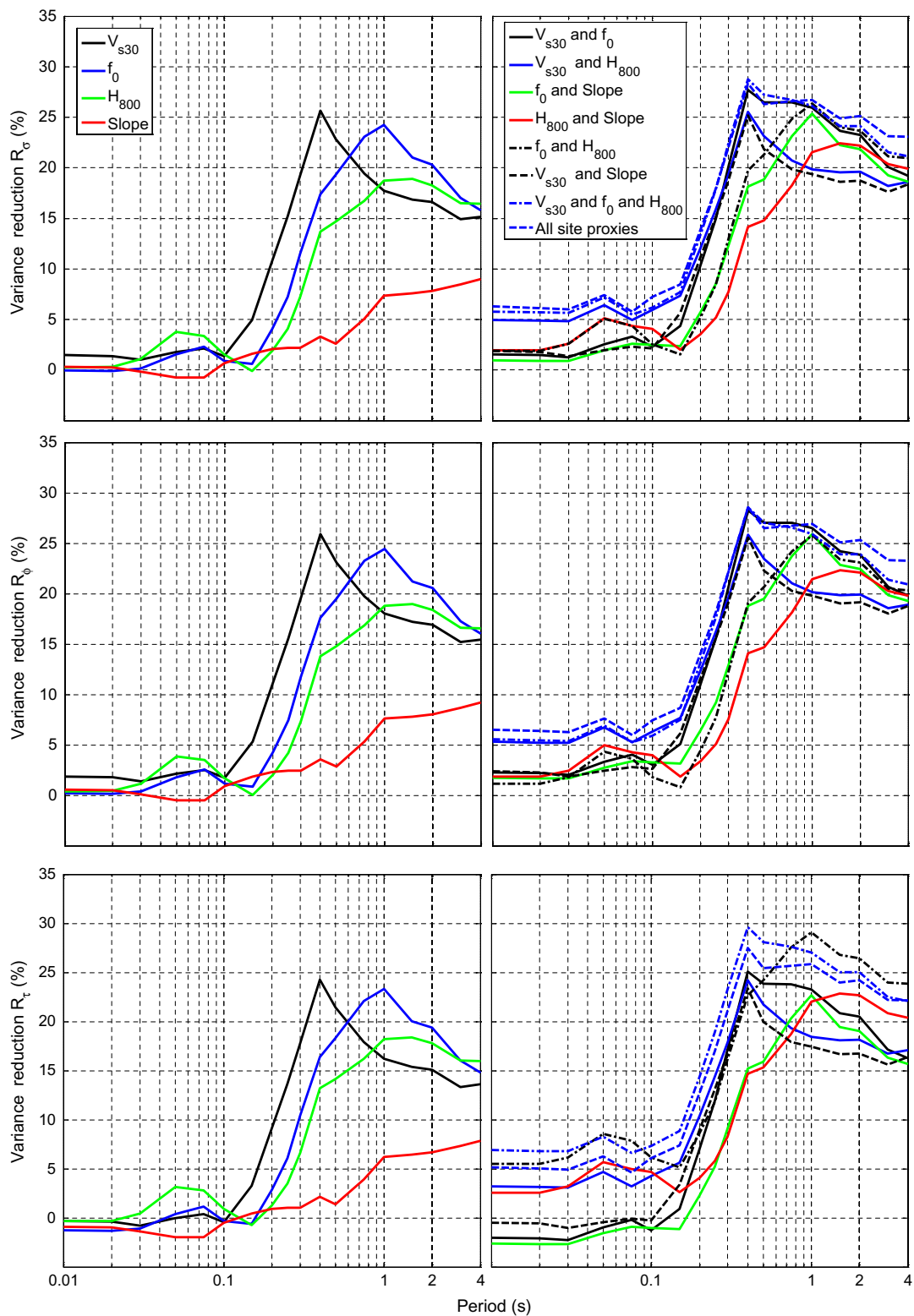


**Fig. 6** Performance of various SCPs in reducing ground-motion aleatory variability. The top frames display the variance coefficient reduction ( $R_\sigma$ ) for the total standard deviation  $\sigma$ . The middle frames illustrate the variance coefficient reduction ( $R_\phi$ ) of the within-event standard deviation  $\phi$ . The bottom frames show the variance coefficient reduction ( $R_\tau$ ) of the between-event standard deviation  $\tau$ . In the left frames (for top, middle and bottom frames), we use four ANN models with one SCP measured  $V_{s30}$  or  $f_0$ ,  $H_{800}$  and slope. In the right frames (for top, middle and bottom frames), we show  $R_\sigma$ ,  $R_\phi$  and  $R_\tau$  for the eight ANN models with two-SCP, three-SCP and four-SCP configurations

**Table 3 Variation reduction in the variance ( $R_v$ ) in % for the 12 ANN models for PGA, PGV and at  $T = [0.2, 0.5, 1.0, 2.0]$  s**

Ground-motion parameters ( $\log_{10}$ )	One SCP ( $\log_{10}$ )			Two SCPs ( $\log_{10}$ )			Three SCPs ( $\log_{10}$ )			Four SCPs ( $\log_{10}$ )		
	$V_{530}$	$f_0$	$H_{800}$ Slope	$(V_{530}, f_0)$	$(V_{530}, H_{800})$	$(f_0, \text{slope})$	$(H_{800}, \text{slope})$	$(f_0, H_{800})$	$(V_{530}, \text{slope})$	$(V_{530}, f_0, H_{800})$	$(V_{530}, f_0, H_{800}, \text{slope})$	
PGA	1.46	0.00	0.28 0.33	1.50	4.88	0.97	1.94	1.88	1.89	5.73	6.23	
PGV	13.44	8.26	5.08 4.00	13.97	13.83	10.07	7.37	9.09	14.27	16.03	16.70	
0.2 s	10.78	4.04	1.88 2.09	10.35	12.02	5.72	3.53	5.17	11.18	13.41	13.87	
0.5 s	22.81	19.31	14.69 2.58	26.49	23.12	18.86	14.79	21.32	21.85	27.21	26.32	
1 s	17.72	24.27	18.72 7.35	25.96	19.87	25.34	21.55	26.36	19.37	26.13	26.72	
2 s	16.60	20.33	18.28 7.82	23.26	19.61	21.85	22.20	23.66	18.72	24.12	25.13	

dependency with a slight trade-off between source- and site-related residuals has already been observed and cannot be avoided (e.g. Ktenidou et al. 2017).

Another parameter used in ANN approach to measure the relevancy of each explanatory variable (and therefore of each single SCP or SCP pair) is the total percentage of synaptic weights  $P$ . As explained in Derras et al. (2012) and Derras et al. (2014), these synaptic weights  $P$  can be estimated from the weights allocated to each input variable in each connection to the hidden layer and provide a measure of the relative, overall importance of the individual explanatory variables, averaged for all the output ground-motion parameters (thus, here, over the whole frequency range 0.01–4 s). They have been computed according to the procedure detailed in Derras et al. (2014, Equation 4), for the 11 ANN models. Tables 4 and 5 list the  $P$  values (in %) for each input variable. As expected from the data distribution, the most efficient parameter in reducing the variance of response spectra is the  $R_{JB}$  distance (synaptic weight around 40–51%), followed directly by the earthquake magnitude  $M_w$  (around 27–36%). The  $P$  values associated with the site term range from 7 to 31%. However, focal depth does not have a great importance ( $P_{Depth} \cong 6$ ).

When only one SCP is considered, the largest SCP weights correspond to  $V_{S30}$  (around 19%) and  $H_{800}$  ( $\cong 18\%$ ), while the smallest corresponds to the slope

( $P_{slope} = 7\%$ ). For the twin-SCP models, the best pair is ( $V_{S30}, H_{800}$ ) with  $P = 25\%$ . The [ $f_0$ , slope] pair also performs well with  $P = 21\%$ . This ranking is similar to the ranking obtained from the analysis of aleatory variabilities discussed above if we consider the whole period range.

As in the aleatory variability analysis described above, the “all proxies” model is considered for comparison. The total synaptic weight of SCPs reaches 31%, which decomposes in individual synaptic weights for each SCP ranking as for the synaptic weight of one-SCP models: the largest one is  $P_{V_{S30}}$ , followed by  $P_{f_0}$  and  $P_{H_{800}}$ , the poorest one is associated with the slope ( $P_{Slope} = 3\%$ ). When the number of SCP increases, the increase in the SCP weight is associated first with a decrease in the magnitude and  $R_{JB}$  weights (from one SCP to two SCPs), while the relative importance of the focal depth (from two SCPs to four SCPs) is 5–6%: the importance of focal depth is not affected by the site described, while  $R_{JB}$  and  $M_w$  obviously remain key parameters.

**Impact of the various SCPs on median ground-motion models**

As discussed above, the nature of SCP has a noticeable effect on the ground-motion aleatory variability. We investigate here their impact on the median estimates, through a comparison of the four one-SCP ANN and six two-SCP ANN models. Figure 7 displays the distance dependence of the spectral acceleration for  $T = 0.0, 0.2$  and  $1.0$  s, for the median magnitude ( $M_w = 5.1$ ), the median focal depth (9 km), and the median values of the various SCPs (i.e.  $V_{S30} = 468$  m/s,  $f_0 = 4.2$  Hz,  $H_{800} = 20$  m and slope = 0.045 m/m, as derived from Fig. 2 and Table 2). Through Fig. 7a, we remark that the site proxy type ( $V_{S30}/f_0/H_{800}/slope$ ) is observed not to have any significant impact on median predictions.

The two-SCP models (Fig. 7b) lead to similar results. All pairs of proxies exhibit very similar median predictions,

**Table 4 Sensitivity of ground-motion models to magnitude, distance and one SCP, as expressed through the total percentages of synaptic weight ( $P$ , %) corresponding to each input parameter**

SCP	$P_{RJB}$	$P_{M_w}$	$P_{Depth}$	$P_{SCP}$
$H_{800}$	43	32	6	18
$V_{S30}$	42	33	6	19
$f_0$	44	33	6	17
Slope	51	36	6	7

**Table 5 Sensitivity of ground-motion models to magnitude, distance, depth, two SCPs and three SCPs, as expressed through the total percentages of synaptic weight ( $P$ , %) corresponding to each input parameter**

SCPs	$P_{RJB}$	$P_{M_w}$	$P_{Depth}$	$P_{SCP1}$	$P_{SCP2}$	$\Sigma P_{SCPs}$		
$V_{S30}, H_{800}$	40	30	5	15	10	25		
$f_0, slope$	42	31	6	17	4	21		
$V_{S30}, f_0$	41	31	6	14	9	23		
$H_{800}, slope$	42	34	6	13	5	18		
$V_{S30}, slope$	41	32	5	19	3	22		
$H_{800}, f_0$	41	30	6	11	12	23		
SCPs	$P_{RJB}$	$P_{M_w}$	$P_{Depth}$	$P_{V_{S30}}$	$P_{f_0}$	$P_{H_{800}}$	$P_{Slope}$	$\Sigma P_{SCPs}$
$V_{S30}, f_0, H_{800}, slope$	37	27	5	11	9	9	2	31

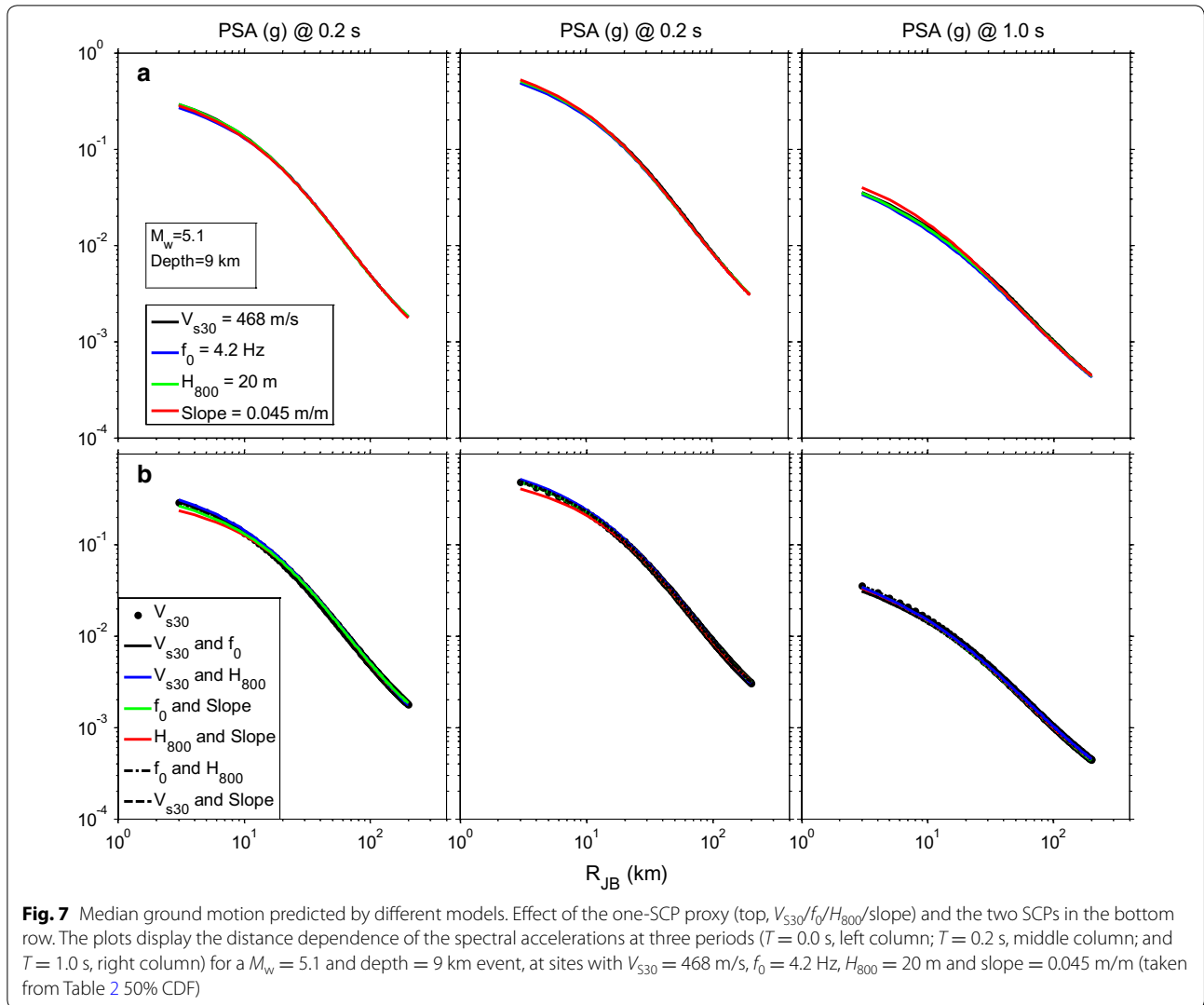


**Fig. 7** Median ground motion predicted by different models. Effect of the one-SCP proxy (top,  $V_{S30}/f_0/H_{800}/\text{slope}$ ) and the two SCPs in the bottom row. The plots display the distance dependence of the spectral accelerations at three periods ( $T = 0.0$  s, left column;  $T = 0.2$  s, middle column; and  $T = 1.0$  s, right column) for a  $M_w = 5.1$  and depth = 9 km event, at sites with  $V_{S30} = 468$  m/s,  $f_0 = 4.2$  Hz,  $H_{800} = 20$  m and slope = 0.045 m/m (taken from Table 2 50% CDF)

especially at short periods ( $T = 0.0$  s,  $T = 0.2$  s and  $T = 1.0$  s). Furthermore, the comparison with the  $V_{S30}$ -SCP model highlights the fact that the type and the number (one SCP or two SCPs) of site proxies have no influence on this median.

**Ground motions for “Extreme” values of site proxies**

Complementary information is provided by the amount of difference in predictions for “extreme” values of the SCP. Figures 8 and 9 display the “soft/stiff” spectral ratio (SR) for various periods ( $T = 0.0, 0.2$  and  $1.0$  s): a consistent definition of “soft” and “stiff” sites was taken for all SCPs, simply by considering the SCP values corresponding to 10 and 90% of the CDF distributions shown in Fig. 2 and listed in Table 2; note, however, that given the negative correlation between  $H_{800}$  and other proxies, the 10% fractile of  $H_{800}$  (i.e. 4 m) has been associated with the

90% fractile of  $V_{S30}$ ,  $f_0$  and slope (i.e. 829 m/s, 11.71 Hz and 0.117 m/m, respectively), and vice versa (i.e. 86 m, 289 m/s, 0.66 Hz and 0.015 m/m, respectively). Figures 8 and 9 display such SR for individual SCP (top) and two-SCP (bottom) cases. SR has the following form:

$$SR(T) = \frac{PSA_{\text{soft}}(T)}{PSA_{\text{stiff}}(T)} \tag{3}$$

Figure 8 shows the sensitivity of the SR amplification factors to  $R_{JB}$  distance, at three different spectral periods (0.0, 0.2 and 1 s), and for a given earthquake scenario ( $M_w = 6$ , depth = 9 km). Besides the trend of site amplification to increase with distance up to 100 km—which is related to nonlinear site response as the loading level is decreasing with increasing distance—the site amplification is found to increase with period, as classically found in most GMPEs. The curves are displayed between

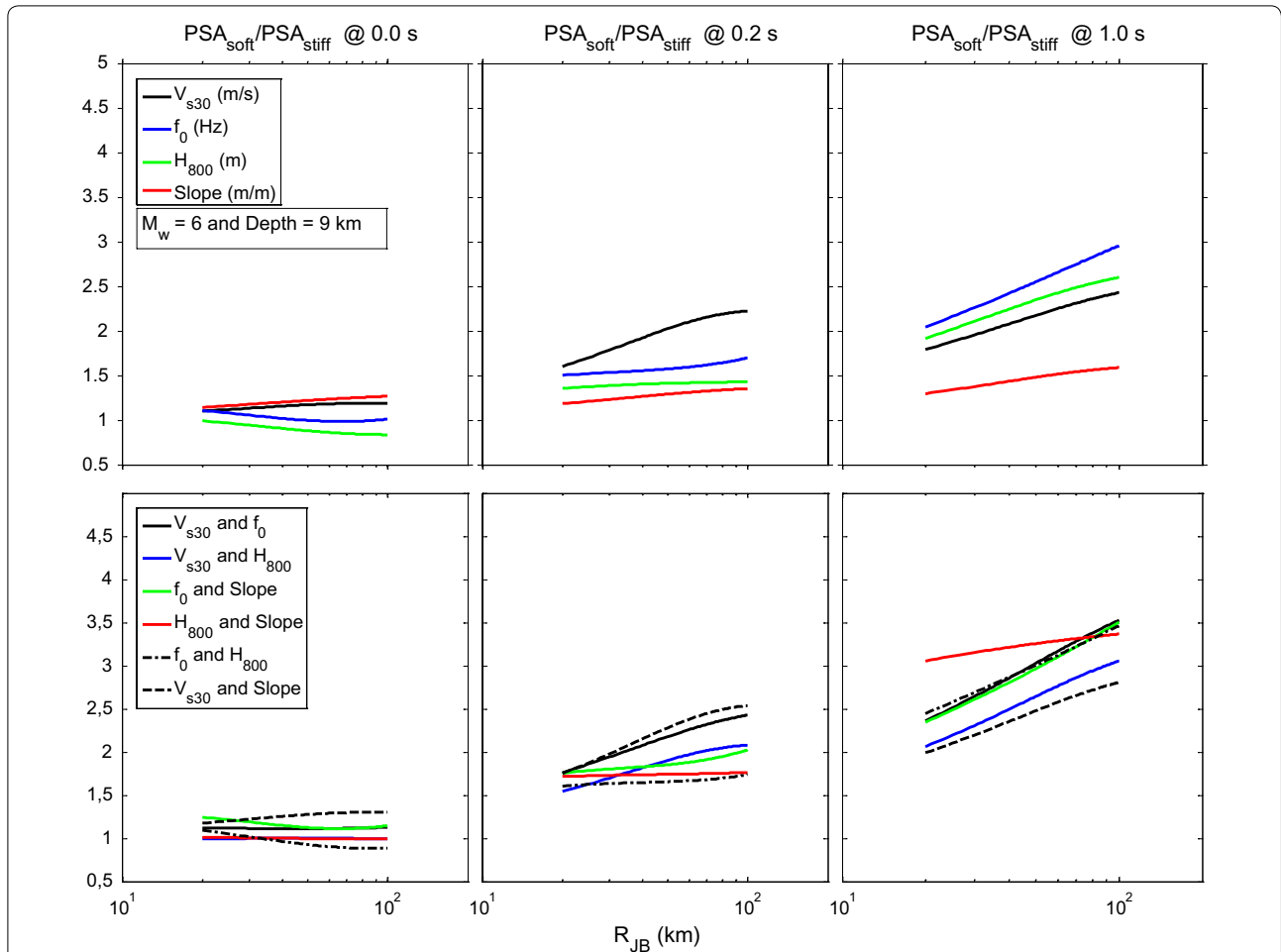


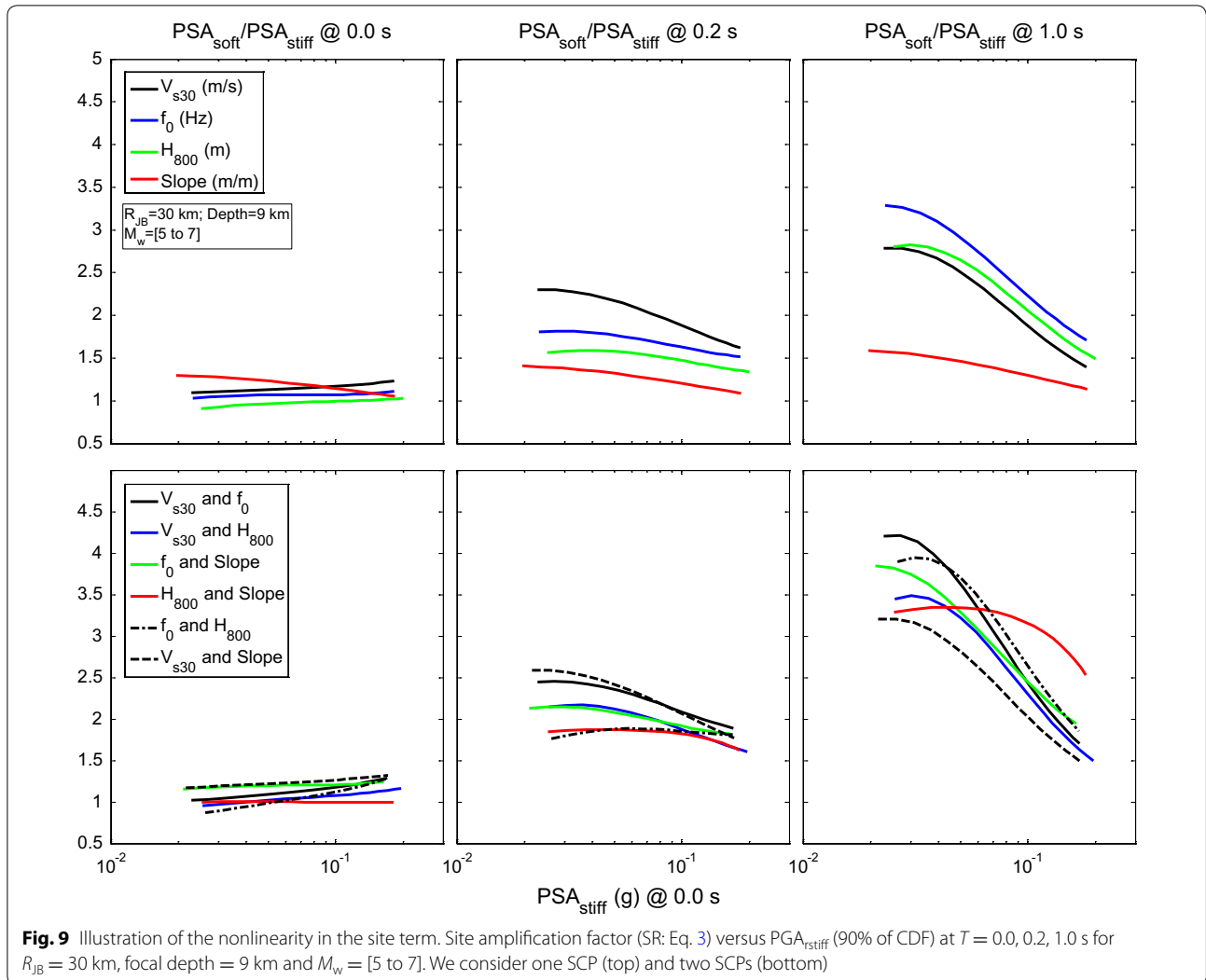
**Fig. 8** Site amplification factor (SR: Eq. 3) versus  $R_{JB}$  at  $T = 0.0, 0.2, 1.0$  s for  $M_w = 6$  and focal depth = 9 km. We consider one SCP (top) and two SCPs (bottom)

[20 and 100] km, considered reliable, since the derived models can hardly be considered reliable for soft and stiff sites at lower distances to 20 km or greater than 100 km (see Fig. 1).  $V_{s30}$  and slope SCPs are found to provide the amplification at short periods (which remains, however, smaller than 27%). The situation is opposite at long period ( $T = 1.0$  s) where the SCP providing the largest amplification is  $f_0$  with amplification ranging from 2 to 3. In addition, it is clear that the site amplification predicted with the slope proxy is not very sensitive to the oscillator period. Another interesting result is that the combination of two proxies significantly increases the “soft/stiff” SR values: the amplification increase ranges from 3% ( $V_{s30}$  to  $V_{s30}$ -slope) at short period, to 12% at intermediate periods, to 16% at long period ( $f_0$  to  $f_0$ - $V_{s30}$ ). The most probable explanation comes from the fact that simultaneously matching 10 and 90% fractiles for a pair of proxies corresponds to less frequent combinations, with more differentiated site conditions, than for a single proxy (as also shown in Fig. 3).

Figure 9 illustrates the SR amplification factors variation versus  $PSA_{stiff}$  at  $T = 0.0$  s (i.e.  $PGA_{stiff}$ ), one of the reference parameters that is commonly used in GMPEs to describe the dependence of the nonlinear site amplification on the loading level. These curves have been established here by considering a given  $R_{JB}$  distance (30 km), a given focal depth (9 km) and a magnitude varying from 5 to 7 with an equal increment 0.125. A closer look at the dependence of soft/stiff amplification factor does indicate a larger amplification level for small stiff motion levels, associated with a significant nonlinearity (i.e. decrease in amplification with increasing loading level at the underlying bedrock). The curves displayed in Fig. 9 call for several comments:

1. The amount of nonlinearity depends both on the considered site proxies and on the oscillator period.
2. Whatever the site proxy, a significant nonlinearity can be observed at long period ( $T = 1$  s), which is a somewhat unexpected result.





3. Among single proxy models, the one using the slope predicts similar nonlinearity whatever the oscillator period, while the “long-period” proxies  $f_0$  and  $H_{800}$  are those who do not predict any significant nonlinearity at short period: the predicted SR is around 1 at  $T = 0.0$  s and around 1.8 to 1.5 at  $T = 0.2$  s. At long period ( $T = 1.0$  s), the SCP providing the largest SR is  $f_0$ , while amplification levels and their nonlinear sensitivity on  $PGA_{stiff}$  are almost similar to  $V_{S30}$  and  $H_{800}$  proxies. This larger amplification factors for the  $f_0$  model at  $T = 1.0$  s might be related to the fact that the “soft” site is characterised by a fundamental frequency of 0.66 Hz: the oscillator frequency (1 Hz) is always larger than the fundamental frequency, and one may thus expect to be systematically in the amplified frequency range, while sites with  $V_{S30} = 289$  m/s or  $H_{800} = 86$  m, with funda-

mental frequencies above 1 Hz (see the last column of Fig. 3), do exist. Correlatively, a larger reduction in the amplification with increasing loading level may be expected if the nonlinear behaviour affects the whole thickness of the soil deposit (see Régnier et al. 2016).

4. Similar observations can be done for the results with two-SCP models. At short period ( $T = 0$  and 0.2 s), the largest amplification and nonlinearity are predicted when using the pair of short-period proxies ( $V_{S30}$ -slope and  $V_{S30}$ - $f_0$ ), while the smallest corresponds to the pair of long-period proxies ( $f_0$ - $H_{800}$  and  $H_{800}$ -slope). At long period ( $T = 1.0$  s), the predicted amplifications and their nonlinear component are less scattered than in the one-SCP case, the pairs including the  $f_0$  proxy predicting, however, slightly larger amplifications.

These results are, however, partial and should not be extrapolated too fast, as they correspond to a specific distance (and focal depth) and use the stiff-site PGA to characterise the loading level.

Figures 10, 11, 12 and 13 are thus intended to check the robustness of the results presented in Fig. 9, considering also other descriptions of the loading level and other distance scenario. Only one-SCP models are considered, successively  $V_{S30}$ ,  $f_0$ ,  $H_{800}$  and slope for Figs. 10, 11, 12 and 13, respectively. In each case, three different distances are considered (30, 50 and 75 km) i.e. in the range where there exist enough data within the [10–90%] fractile range of each SCP, and the variation of the loading level for each distance corresponds to the predictions over the magnitude range [5–7] with an equal increment of 0.125. Three different parameters are considered to characterise the loading level: the PGA on rock or “stiff” site as defined according to the selected site proxy, the spectral acceleration on the same rock or “stiff” site at the oscillator period considered, and finally an estimate of the actual strain at the site: several authors (Idriss, 2011; Chandra et al. 2015, 2016; Guéguen 2016) proposed to use the ratio  $PGV/V_{S30}$  as a proxy to the shear strain, where  $PGV$  is the peak velocity at the site, and it has thus been tested in the present study. In principle, if a loading parameter is relevant for nonlinear behaviour, the dependency of site amplification as a function of this loading parameter should exhibit only a marginal dependency on other parameters such as magnitude, or distance or frequency contents. Analysing Figs. 10, 11, 12 and 13 according to this criterion clearly indicates that the lowest scatter is observed among distance and magnitude scenarios for the loading parameter “ $PSA_{stiff}(T)$ ” (second row), while the largest corresponds to “ $PGA_{stiff}$ ”, especially for the long-period site amplification.

In the light of these results, it turns out that the best ground-motion parameter to be used for the characterisation of the loading level in the nonlinear site amplification term of GMPEs is the spectral ordinate on rock at the considered period; the strain proxy  $PGV/V_{S30}$  may, however, constitute a satisfactory, alternative choice. Another major outcome of this section is the variability of the nonlinear behaviour according to the site proxy selected for the GMPEs: short-period nonlinearity is observed preferably with short-period proxies ( $V_{S30}$  and slope) and disappears when using  $H_{800}$ .

### Summary and conclusions

The application of neural networks approach to a KiK-net data set offered the possibility to test the performance of various site-condition proxies to reduce the aleatory variability in GMPEs. The four available SCPs are  $V_{S30}$  and  $H_{800}$  (both derived from downhole measurements),

$f_0$  (the fundamental frequency derived from H/V ratios and surface/downhole spectral ratios), and the slope derived from DEM data, which has been proposed as a proxy to  $V_{S30}$  values. A total of 16 neural network models were derived to describe the dependence of response spectra ordinates on moment magnitude  $M_w$ , Joyner and Boore distance  $R_{JB}$ , focal depth and various combinations of SCPs: one without any SCP which provides the “reference case”, four with each single SCP, six with the six possible pairs of SCPs [ $V_{S30}-f_0$ ], [ $V_{S30}-H_{800}$ ], [ $f_0$ -slope], [ $H_{800}$ -slope], [ $V_{S30}$ -slope] and [ $f_0-H_{800}$ ], four with the four possible combinations of three SCPs, and one with all SCPs considered simultaneously.

When only one SCP is used, the largest reduction in aleatory variability with respect to the “reference case” is found to be provided by  $V_{S30}$  at short-to-intermediate periods ( $T \leq 0.6$  s), and by  $f_0$  or  $H_{800}$  at longer periods. Among the four SCPs, the parameter “slope” is thus found to provide the worst performance when considered alone. However, when SCP pairs are considered, comparable performance is found whatever the pair of proxies. In particular, the “best pairs” are found to be [ $V_{S30}-H_{800}$ ] at short periods and [ $f_0-H_{800}$ ] at long periods, while the “low-cost” pair [ $f_0$ -slope] provides a good compromise over the whole period range [0.1–4 s]. None of the four tested SCPs is thus “optimal” over the whole period range, and all proxies show a poor contribution at high frequencies (>10 Hz).

Otherwise, the site proxy type (slope/ $V_{S30}$ / $H_{800}$ / $f_0$ ) has no influence on the median, and these results indicate that the type of SCP does not really affect the median.

Regarding site amplification,  $V_{S30}$  and slope SCPs are found to provide some differentiation at short periods (0, 0.2 s). At long period,  $H_{800}$  and  $f_0$  are providing the largest differentiation. We showed also that, for this subset of KiK-net data, the soft-to-stiff-site amplifications exhibit a significant nonlinearity, the characteristics of which are, however, tightly linked to the used proxy, and the parameter selected to describe the loading level. The most relevant loading parameter is found to be the spectral acceleration on rock (or “stiff” site) at the considered period, and the worst the rock (or “stiff”) peak acceleration, with a satisfactory behaviour for the strain proxy  $PGV/V_{S30}$ . Nonlinearities are found to be systematically larger at intermediate period (1 s) than at short period (0.2, 0 s). This purely data-driven result is rather intriguing and calls for further checks, such as the use of larger data sets, especially at long periods (for instance, adding recordings from interplate earthquakes), the comparison with the site-specific nonlinearities as defined by the  $RSR_{NL-L}$  ratio introduced by Régnier et al. (2013, 2016), i.e. the ratio between the surface-downhole transfer function obtained for strong motion and the transfer function

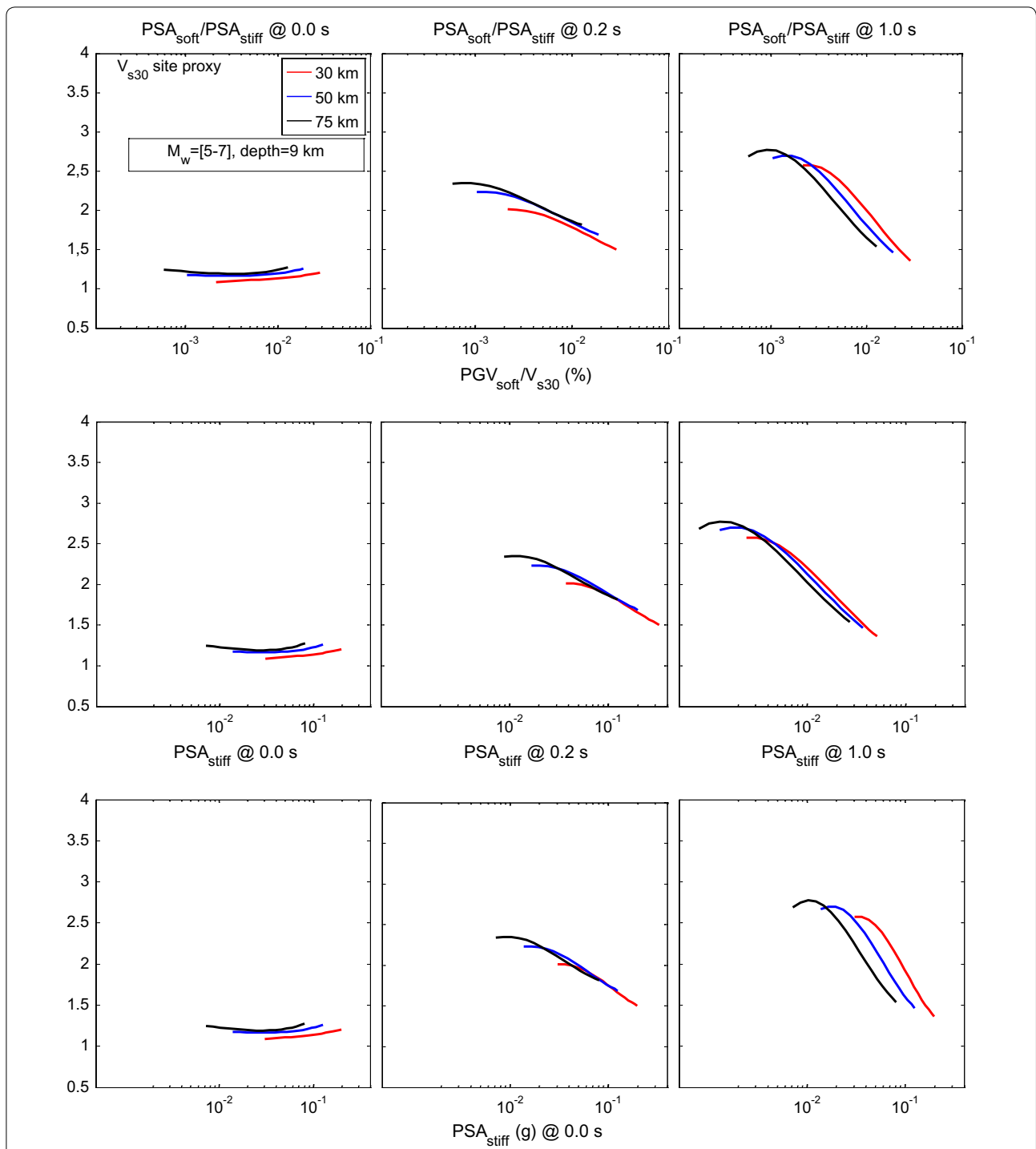
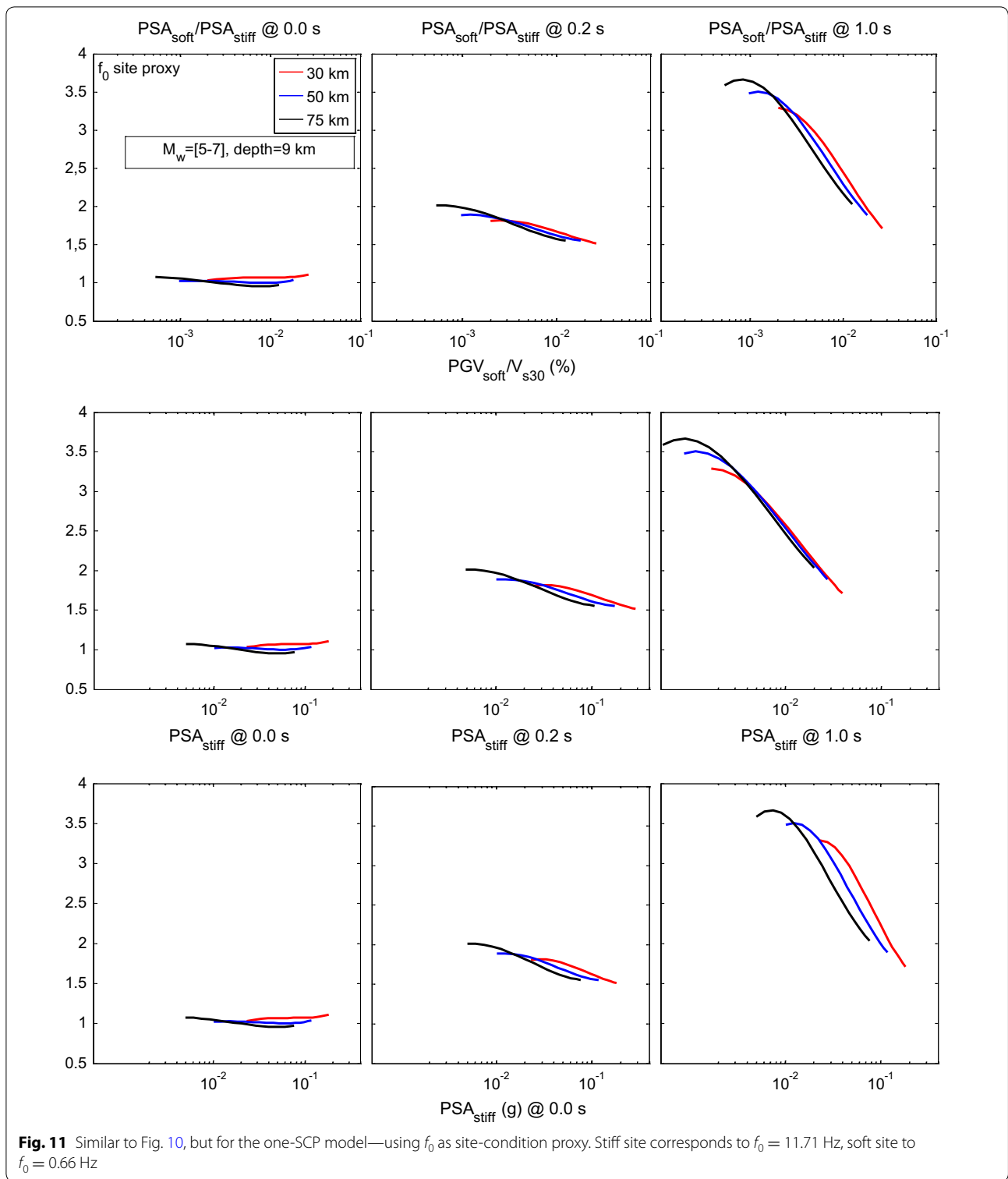


**Fig. 10** Comparison of the NL components of site amplification for different descriptions of the loading level, for the one-SCP ANN model using  $V_{s30}$ . Each panel represents the (soft/stiff) site amplification at a given oscillator period as a function of a loading parameter. The three columns correspond to three different oscillator periods (0, 0.2 and 1.0 s). The three rows correspond to different choices for the loading level: strain proxy  $PGV_{soft}/V_{s30}$  on top, spectral ordinates at the stiff-site  $PSA_{stiff}(T)$  in the middle and  $PSA_{stiff}$  at the 0.0 s (bottom). As shown in Fig. 9, the site amplification factors (SR; Eq. 3) are calculated for three distances: 30 km, 50 km and 75 km, for which the variation of loading level corresponds to magnitude variations between 5 and 7 (for a fixed focal depth equal to 10 km)



derived only for weak motions, and possibly the testing of other, basin-related, site proxies such as  $H_{1100}$  or  $H_{2500}$ . Another important result (which will also have to be investigated further) is the variability of the nonlinear

site response according to the SCP: short-period non-linearity is observed preferably with short-period proxies ( $V_{S30}$  and slope) and disappears when using  $H_{800}$ .

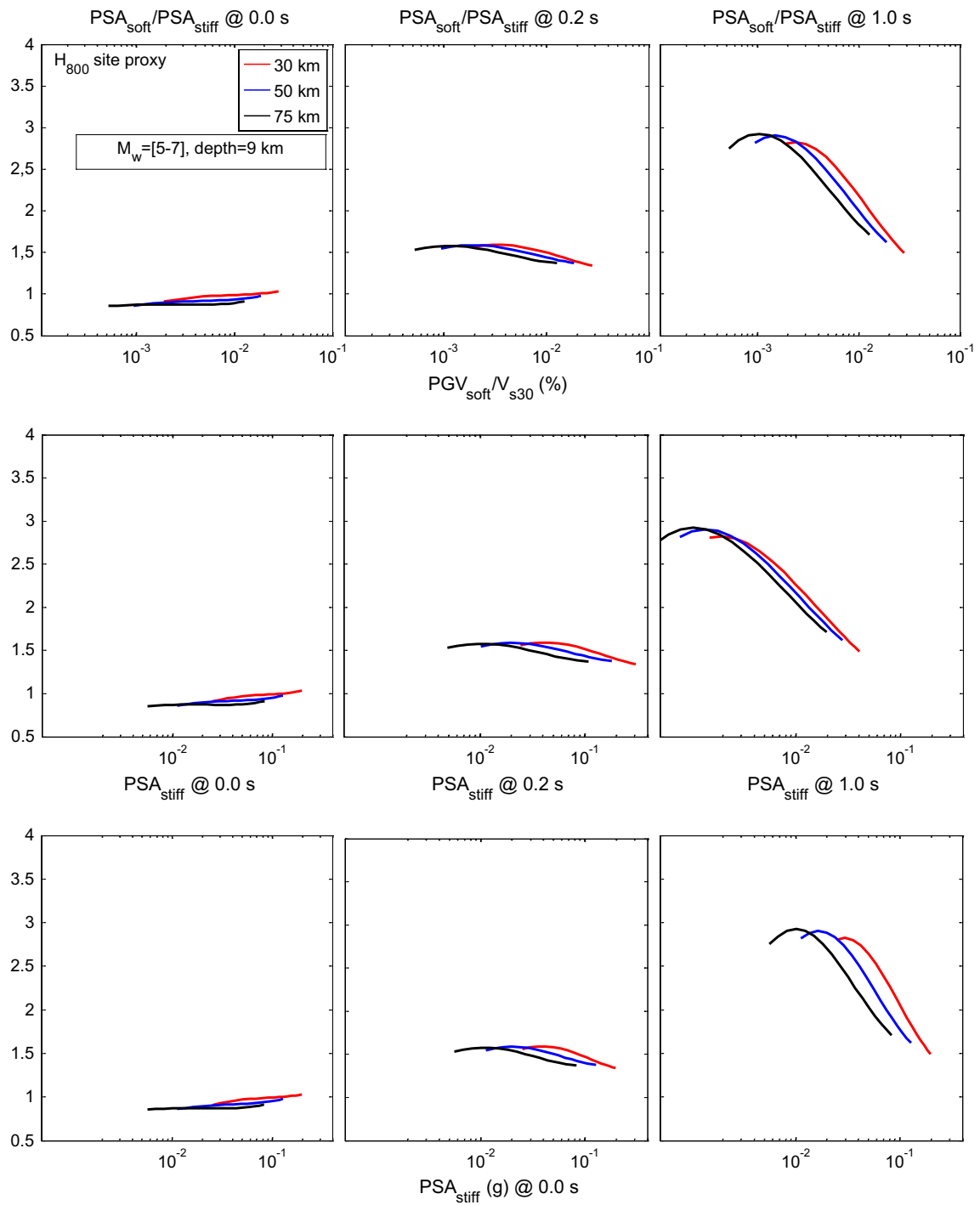


**Fig. 12** Similar to Fig. 10, but for the one-SCP model—using  $H_{800}$  as site-condition proxy. Stiff site corresponds to  $H_{800} = 4$  m, soft site to  $H_{800} = 86$  m



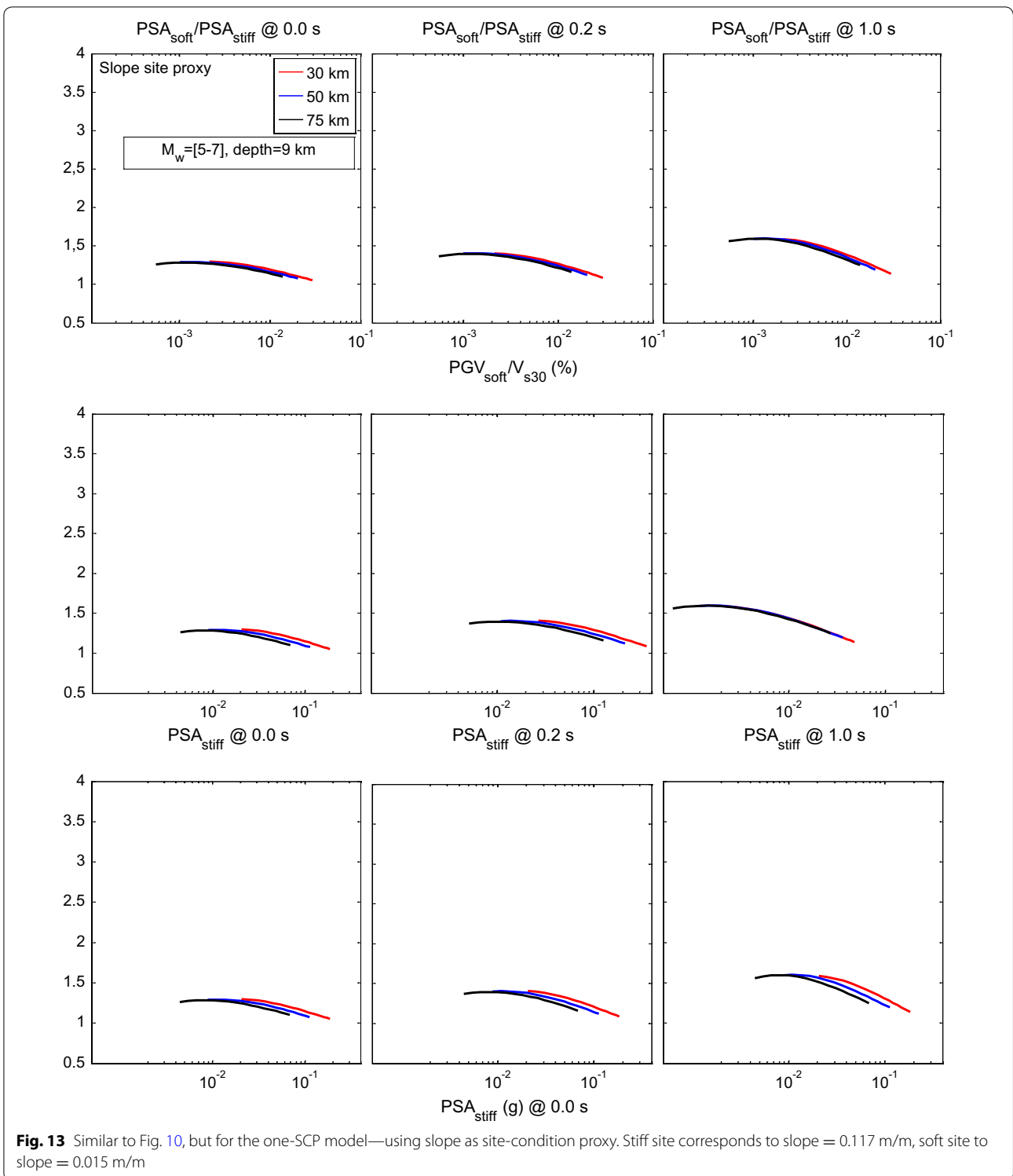


**Fig. 13** Similar to Fig. 10, but for the one-SCP model—using slope as site-condition proxy. Stiff site corresponds to slope = 0.117 m/m, soft site to slope = 0.015 m/m

As these results have been obtained on a specific—though large—data set (subset of KiK-net data, thus probably lacking of very soft sites), they should of course be tested for other data sets; the four SCPs are, however, rarely available simultaneously.

#### Abbreviations

SCP: site-condition proxy;  $V_{S30}$ : time-averaged shear-wave velocity in the top 30 m;  $H_{800}$ : depth beyond which  $V_s$  exceeds 800 m/s;  $f_0$ : fundamental resonance frequency; Slope: topographical slope; DEM: digital elevation models; PGA: peak ground acceleration; PGV: peak ground velocity; PSA: pseudo-spectral acceleration; GMPs: ground-motion prediction equations; ANN: artificial neural network;  $M_w$ : moment magnitude;  $R_{JB}$ : Joyner and Boore distance; Depth: focal depth; CDF: cumulative distribution function;  $R$ : coefficient of correlation;  $\tau$ : between-event standard deviation;  $\phi$ : within-event standard deviation;  $\sigma$ : total standard deviation;  $R_1$ : between-event variance reduction coefficient;  $R_w$ : within-event variance reduction coefficient;  $R_G$ : total variance reduction coefficient; P: total percentage of synaptic weights; SR: spectral ratio.

#### Authors' contributions

Most of the scientific and technical work has been carried out by BD, under the scientific supervision of P-YB and FC. The redaction has been shared among the three authors. All authors read and approved the final manuscript.

#### Author details

<sup>1</sup> Risk Assessment and Management Laboratory (RISAM), Abou Bekr Belkaïd University, BP 230, 13048, Chetouane, Tlemcen, Algeria. <sup>2</sup> Department of Civil Engineering and Hydraulics, Dr Moulay Tahar University, BP 138, 20000, Ennasr, Saïda, Algeria. <sup>3</sup> Institut des Sciences de la Terre (ISTerre), IFRSTAR, CNRS, IRD, Bâtiment OSUG C, Grenoble-Alpes University, CS 40700, 38058 Grenoble Cedex 9, France. <sup>4</sup> Section 2.6 Hazard and Stress Field, GFZ German Research Center for Geoscience, Telegrafenberg, 14473 Potsdam, Germany. <sup>5</sup> Institute of Earth and Environmental, University of Potsdam, Potsdam, Germany.

#### Acknowledgements

The authors thank Julie Régnier and Héroïse Cadet for their generous help and which provided us the  $f_0$  of the KiK-net database. We acknowledge the support from the TASSILI program, the sinaps@ project (<http://www.institut-seism.fr/projets/sinaps/>). We also thank an anonymous reviewer for their constructive criticism and comments that helped us to improve this study. The authors would like to thank Haitham Dawood and Adrian Rodriguez-Marek for providing high-quality data.

#### Competing interests

The authors declare that they have no competing interests.

#### Data and resources

PSA,  $V_{S30}$  and  $H_{800}$  used in this study were collected from the KiK-net website <https://datacenterhub.org/resources/272>. Slope have been collected and disseminated by the "The Pacific Earthquake Engineering Research Center" at <http://peer.berkeley.edu/ngawest2/databases/>.  $f_0$  from Régnier et al. (2013).

#### Publisher's Note

Springer Nature remains neutral with regard to jurisdictional claims in published maps and institutional affiliations.

Received: 18 January 2017 Accepted: 11 September 2017

Published online: 22 September 2017

#### References

Abrahamson NA, Youngs RR (1992) A stable algorithm for regression analyses using the random-effects model. *Bull Seismol Soc Am* 82(1):505–510

Akaike H (1973) Information theory and an extension of the maximum likelihood principle. In: *Proceedings of the 2nd international symposium on information theory*, vol 1, pp 267–281. Budapest, Hungary

Al Atik L, Abrahamson N, Bommer JJ, Scherbaum F, Cotton F, Kuehn N (2010) The variability of ground motion prediction models and its components. *Seismol Res Lett* 81(5):794–801

Allen TI, Wald DJ (2009) On the use of high-resolution topographic data as a proxy for seismic site conditions ( $V_{S30}$ ). *Bull Seismol Soc Am* 99:935–943

Ancheta TD, Darragh RB, Stewart JP, Seyhan E, Silva WJ, Chiou S-J, Wooddell KE, Graves RW, Kottke AR, Boore DM, Kishida T, Donahue JL (2014) NGA-West 2 database. *Earthq Spectra* 30(3):989–1005

Bard P-Y, Cadet H, Endrun B, Hobiger M, Renalier F, Theodulidis N, Ohrnberger M, Fäh D, Sabetta F, Teves-Costa P, Duval A-M, Cornou C, Guillier B, Wathelet M, Savvaidis A, Köhler A, Burjanek J, Poggi V, Gassner-Stamm G, Havenith HB, Hailemichael S, Almeida J, Rodrigues I, Veludo I, Lacave C, Thomassin S, Kristekova M (2010) From non-invasive site characterisation to site amplification: Recent advances in the use of ambient vibration measurements. In: *Garevski M, Ansal A (eds) Earthquake engineering in Europe. Geotechnical, geological, and earthquake engineering books*, New York, pp 105–123

Boore DM (2005) On pads and filters: processing strong-motion data. *Bull Seismol Soc Am* 95(2):745–750

Boore DM, Joyner WB, Fumal TE (1993) Estimation of response spectra and peak accelerations from western North American earthquakes: an interim report, part 2. U.S. Geological Survey Open-File Report 94-127

Boore DM, Joyner WB, Fumal TE (1997) Equations for estimating horizontal response spectra and peak acceleration from western North American earthquakes: a summary of recent work. *Seismol Res Lett* 68(1):128–153

Borcherdt RD (1994) Estimates of site-dependent response spectra for design (methodology and justification). *Earthq Spectra* 10(4):617–653

Brillinger DR, Preisler HK (1985) Further analysis of the Joyner-Boore attenuation data. *Bull Seismol Soc Am* 75:611–614

Cadet H, Bard P-Y, Duval A-M, Bertrand E (2011) Site effect assessment using KiK-net data: part 2—site amplification prediction equation based on  $f_0$  and  $V_{sz}$ . *Bull Earthq Eng* 10(2):451–489

Campbell KW (1989) Empirical prediction of near-source ground motion for the Diablo Canyon power plant site. San Luis Obispo County, California, U.S. Geological Survey Open-File Report 89-484

Campbell KW (1993) Empirical prediction of near-source ground motion from large earthquakes. In: *Proceedings international workshop on earthquake hazards and large dams in the Himalaya*, January 15–16, New Delhi, India

Chandra J, Gueguen P, Steidl JH, Bonilla LF (2015) In-situ assessment of the G-y curve for characterizing the nonlinear response of soil: application to the Garner Valley downhole array (GVDA) and the wildlife liquefaction array (WLA). *Bull Seismol Soc Am* 105(2A):993–1010

Chandra J, Gueguen P, Bonilla LF (2016) PGA-PGV/ $V_s$  considered as a stress-strain proxy for predicting nonlinear soil response. *Soil Dyn Earthq Eng* 85:146–160

Chiou B-SJ, Youngs RR (2008) An NGA model for the average horizontal component of peak ground motion and response spectra. *Earthq Spectra* 24(1):173–215

Chiou B-SJ, Youngs RR (2014) Update of the Chiou and Youngs NGA ground motion model for average horizontal component of peak ground motion and response spectra. *Earthq Spectra* 30:1117–1153

Choi Y, Stewart JP (2005) Nonlinear site amplification as function of 30 m shear wave velocity. *Earthq Spectra* 21(1):1–30

Dawood HM, Rodriguez-Marek A, Bayless J, Goulet C, Thompson E (2015) NEES: The KiK-net database processed using an automated ground motion processing protocol. <https://datacenterhub.org/resources/272>

Dawood HM, Rodriguez-Marek A, Bayless J, Goulet C, Thompson E (2016) A flatfile for the KiK-net database processed using an automated protocol. *Earthq Spectra* 32(2):1281–1302

Demuth H, Beale M, Hagan M (2009) *Neural Network Toolbox™6: user's guide*. MATLAB. The MathWorks Inc, Natick

Derras B, Bard P-Y, Cotton F, Bekkouche A (2012) Adapting the neural network approach to PGA prediction: an example based on the KiK-net data. *Bull Seismol Soc Am* 102(4):1446–1461

Derras B, Bard P-Y, Cotton F (2014) Towards fully data-driven ground-motion prediction models for Europe. *Bull Earthq Eng* 12(1):495–516

Derras B, Bard P-Y, Cotton F (2016) Site-conditions proxies, ground-motion variability and data-driven GMPs insights from NGA-West 2 and RES-ORCE datasets. *Earthq Spectra* 32(4):2027–2056

- Guéguen P (2016) Predicting nonlinear site response using spectral acceleration vs  $PGV/V_{s30}$ : a case history using the Volvi-test site. *Pure appl Geophys* 173(6):2047–2063
- Haghshenas E, Bard P-Y, Theodulidis N, SESAME WP04 Team (2008) Empirical evaluation of microtremor H/V spectral ratio. *Bull Earthq Eng* 6(1):75–108
- Hayashida T, Tajima F (2007) Calibration of amplification factors using KiK-net strong-motion records: toward site effective estimation of seismic intensities. *Earth Planets Space* 59:1111–1125. doi:10.1186/BF03352054
- Idriss IM (2011) Use of  $V_{s30}$  to represent local site condition. In: Proceedings of the 4th IASPEI/IAEE international symposium. Effects of source geology on seismic motion, August 23–26, California, USA
- Ktenidou O-J, Roumelioti Z, Abrahamson N, Cotton F, Pitilakis K, Hollender F (2017) Understanding single-station ground motion variability and uncertainty (sigma): lessons learnt from EUROSEISTEST. *Bull Earthq Eng*. doi:10.1007/s10518-017-0098-6
- Luzi L, Puglia R, Pacor F, Gallipoli MR, Bindi D, Mucciarelli M (2011) Proposal for a soil classification based on parameters alternative or complementary to  $V_s$ , 30. *Bull Earthq Eng* 9(6):1877–1898
- Mucciarelli M (1998) Reliability and applicability of Nakamura's technique using microtremors: an experimental approach. *J Earthq Eng* 2(04):625–638
- Régnier JH, Cadet LF, Bonilla LF, Bertrand E, Semblat J-F (2013) Assessing nonlinear behavior of soils in seismic site response: statistical analysis on KiK-net strong-motion data. *Bull Seismol Soc Am* 103(3):1750–1770
- Régnier J, Cadet H, Bard P-Y (2016) Empirical quantification of the impact of non-linear soil behaviour on site response. *Bull Seismol Soc Am* 106(4):1710–1719
- Sadigh K, Chang C-Y, Egan JA, Makdisi FI, Youngs RR (1997) Attenuation relationships for shallow crustal earthquakes based on California strong motion data. *Seismol Res Lett* 68(1):180–189
- Seyhan E, Stewart JP, Ancheta TD, Darragh RB, Graves RW (2014) NGA-West2 site database. *Earthq Spectra* 30(3):1007–1024
- Shanno DF, Kettler PC (1970) Optimal conditioning of quasi-Newton methods. *Math Comput* 24:657–664
- Wald DJ, Allen TI (2007) Topographic slope as a proxy for seismic site conditions and amplifications. *Bull Seismol Soc Am* 97(5):1379–1395

Submit your manuscript to a SpringerOpen<sup>®</sup> journal and benefit from:

- Convenient online submission
- Rigorous peer review
- Open access: articles freely available online
- High visibility within the field
- Retaining the copyright to your article

---

Submit your next manuscript at ► [springeropen.com](http://springeropen.com)

---